Steel and Composite Structures, *Vol. 31, No. 6 (2019) 591-600*
DOI: https://doi.org/10.12989/scs.2019.31.6.591

Vibration characteristic analysis of high-speed railway simply supported beam bridge-track structure system

Lizhong Jiang [1,2a], Yulin Feng [1,2b], Wangbao Zhou [*1,2] and Binbin He [3c]

[1] *School of Civil Engineering, Central South University, Changsha 410075, China*
[2] *National Engineering Laboratory for High Speed Railway Construction, Changsha 410075, China*
[3] *University of Chinese Academy of Sciences, Beijing 100049, China*

(*Received August 30, 2018, Revised April 29, 2019, Accepted May 12, 2019*)

Abstract. Based on the energy-variational principle, a coupling vibration analysis model of high-speed railway simply supported beam bridge-track structure system (HSRBTS) was established by considering the effect of shear deformation. The vibration differential equation and natural boundary conditions of HSRBTS were derived by considering the interlayer slip effect. Then, an analytic calculation method for the natural vibration frequency of this system was obtained. By taking two simply supported beam bridges of high-speed railway of 24 m and 32 m in span as examples, ANSYS and MIDAS finite-element numerical calculation methods were compared with the analytic method established in this paper. The calculation results show that two of them agree well with each other, validating the analytic method reported in this paper. The analytic method established in this study was used to evaluate the natural vibration characteristics of HSRBTS under different interlayer stiffness and length of rails at different subgrade sections. The results show that the vertical interlayer compressive stiffness had a great influence on the high-order natural vibration frequency of HSRBTS, and the effect of longitudinal interlayer slip stiffness on the natural vibration frequency of HSRBTS could be ignored. Under different vertical interlayer stiffness conditions, the subgrade section of HSRBTS has a critical rail length, and the critical length of rail at subgrade section decreases with the increase in vertical interlayer compressive stiffness.

Keywords: timoshenko; high-speed railway; interlayer slip; shear deformation; critical length

1. Introduction

High-speed railways play an increasingly prominent role in the transportation system, significantly improving the transportation capability and promoting the economic development of the regions along the railway line. Track structure is the supporting structure for the running of high-speed trains, guaranteeing the safe running and comfort of high-speed trains. Analysis of the variation characteristics of track structure is a very important research topic in the railway engineering field. On one hand, trains running with a high speed induce a dynamic impact on the track structure, influencing their working state and service life. On the other hand, the vibration of track structure in turn affects the running stability and safety of trains (Zhang *et al*. 2016).

At present, extensive studies have been conducted on the variation characteristics of track structures (Connolly *et al*. 2016). Kimani and Kaewunruen (2017) investigated the free vibration of a precast steel concrete composite railway track slabs. The slender nature of the slab panel due to its reduced depth of construction makes it susceptible to vibration problems. Free vibration analysis of the track slab has been carried out using ABAQUS. Both eigen-frequencies and eigenmodes have been extracted using the Lanczos method. However, the variation characteristics of bridge subgrade track structure system have been rarely studied by considering them simultaneously. Lei and Rose (2008) presented a methodology for analyzing track vibration using Fourier transform technique. Then, based on the model that was used to conduct the vibration analysis of a vehicle-track subgrade coupling system, Lei and Zhang (2011) also presented a new type of slab track element. Luo and Lei (2014) presented a hybrid method combining finite-element method and statistical energy analysis for predicting the steady-state response of vibro-acoustic systems. Based on the structural characteristics of vehicle CRTS II ballastless track-bridge system, a hybrid method of vehicle-track-bridge elements was presented. Based on the vehicle-track coupling dynamics methodology, Yang and He (2012) established a vibration model. This was used to analyze the vibration characteristics of trapezoidal-sleeper track systems under subway vehicles. Then, Yang *et al*. (2016) developed a high-speed train track subgrade vertical coupled dynamic model in the frequency domain. Combined with the pseudo-excitation method, a solution of random dynamic response is presented. Yang and Yau (2017) provided a complete coverage for the train-induced and bridge-induced resonances of a train-bridge system

*Corresponding author, Ph.D., Professor,
E-mail: zhouwangbao@163.com
[a] Ph.D., Professor, E-mail: lzhjiang@csu.edu.cn
[b] Ph.D. Student, E-mail: fylin119@csu.edu.cn
[c] Ph.D., E-mail: hebinbin@lzb.ac.cn

http://www.techno-press.org/?journal=scs&subpage=6
ISSN: 1229-9367 (Print), 1598-6233 (Online)

using both the analytic and finite-element approaches, focusing on the interacting resonant mechanism between the two subsystems of moving train and bridge.

Romero *et al*. (2012) analyzed the dynamic vehicle-track-bridge-soil interaction in high-speed railway lines. The analysis was carried out using a general and fully three-dimensional multi-body-finite element- boundary element model, formulated in the time domain to predict vibrations owing to the train passage over the bridge. Based on the tests and dynamic receptance method, a steady analytic model of vehicle-track coupled vibration in frequency domain, considering the effect of multiple wheels, was first established by Zhu *et al*. (2016) and Li *et al*. (2018). Hu *et al*. (2016) established an elaborated 2.5D track-embankment-ground finite-element model to study the dynamic response of a track structure under a series of train wheel axle loads. Liu *et al*. (2018) established a spatial model integrating rails-steel truss arch bridges-subgrades in high-speed railway lines, and discussed the natural vibration characteristics of steel truss arch bridges considering the effect of track constraint. Gao *et al*. (2016) formulated a 3D dynamic track-subgrade interaction model to evaluate and predict the track and soil dynamic responses under different train speeds. This was then validated at a range of train speeds. A dynamic analysis of an elevated railway track with surface foundations was carried out by Bucinskas *et al*. (2016), the effects of structure-soil- structure interaction on the dynamic behavior of surrounding soil surface were evaluated. Subgrade and bridge are connected by track, and the connection mode between track and subgrade is the same as that between track and bridge (Xie *et al*. 2012). The studies of the length of rail at subgrade section on both sides of the bridge are not clear, some studies have shown when the length of rail at subgrade section is more than 200m, the value of the length has little influence on the calculation results (Toyooka *et al*. 2005).

In a word, the variation characteristics of a track system are of great theoretical significance to guarantee the long-term and safe running of high-speed trains and have practical significance in this engineering field. Compared with the Euler beam model, the Timoshenko beam model can consider the effect of both rotational inertia and shear deformation of rail (Zhai 2002, Hou *et al*. 2015, Bian *et al*. 2016). At present, only a few studies have been reported on the variation characteristics of bridge-track system (Sun 2014) based on Timoshenko beam model. In this paper, based on the energy-variational principle, a theoretical model for HSRBTS coupling variation was established by considering the effect of shear deformation and rotational inertia, and an analytic calculation method for HSRBTS was obtained by considering the interlayer slip effect. Finally, the analytic method established in this paper was used to study the natural vibration characteristics of HSRBTS under different interlayer stiffness and length of rails in different subgrade sections, and the critical length of rails in the subgrade section of HSRBTS was calculated.

2. Theoretical analysis of vibration characteristics of HSRBTS

2.1 Interlayer stress analysis of HSRBTS

Fig. 1 shows the constructional drawing of HSRBTS. For simplification, the rail was divided into three parts to conduct the stress analysis: rail I at subgrade section, rail II at bridge section, and rail III at subgrade section. The filling soil grade of subgrade is assumed to be appropriate, which has good strength and stability. The fasteners between the rail and bridge, and between the rail and the subgrade are all assumed to be evenly distributed (Lai and Ho 2016, Siekierski 2016, Kun *et al*. 2017).

The vertical interlayer compressive stress between subgrade and rail I and rail III can be expressed as follows

$$\vartheta_1(x,t)=k_1 w_1(x,t), \qquad \vartheta_3(x,t)=k_3 w_3(x,t) \tag{1}$$

where, w_1 (x, t) and w_3 (x, t) are the vertical deflection of rail I and rail III, respectively; k_1 and k_3 are the vertical interlayer compressive stiffness between rail I and rail III, and subgrade.

The longitudinal interlayer relative slip between rail I and rail III, and subgrade can be expressed as follows

$$\zeta_1(x,t)=h_r\theta_1(x,t) \qquad \zeta_3(x,t)=h_r\theta_3(x,t) \tag{2}$$

The longitudinal interlayer shear stress between rail I and rail III, and subgrade can be expressed as follows

$$\begin{aligned}\varsigma_1&=k_{s1}\zeta_1(x,t)=k_{s1}h_r\theta_1(x,t),\\ \varsigma_3&=k_{s3}\zeta_3(x,t)=k_{s3}h_r\theta_3(x,t)\end{aligned} \tag{3}$$

where, h_r is half of the transverse cross-section height of the rail; θ_1 (x, t) and θ_3 (x, t) are the cross-section angles of rail I and rail III, respectively; k_{s1} and k_{s3} are the longitudinal interlayer slip stiffness between rail I and rail III, and subgrade.

The vertical compressive stress between bridge and rail II can be expressed as follows

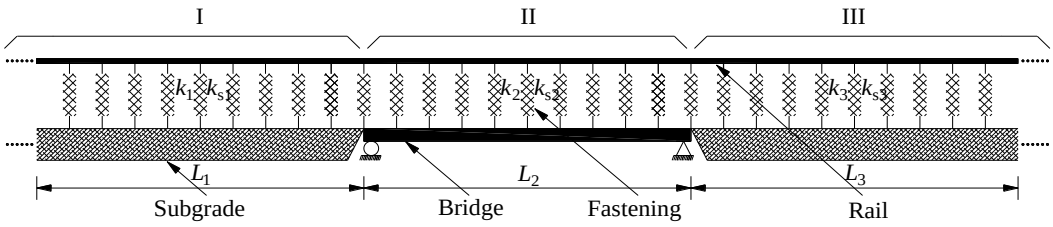

Fig. 1 Constructional drawing of HSRBTS

$$\vartheta_2(x,t)=k_2\left[w_2(x,t)-w_4(x,t)\right] \tag{4}$$

where, w_2 (x, t) and w_4 (x, t) are the vertical deflection between rail II and bridge; k_2 is the vertical interlayer compressive stiffness between rail II and bridge.

The longitudinal interlayer relative slip between rail II and bridge can be expressed as follows

$$\zeta_2(x,t)=\left(h_r\theta_2(x,t)+h_b\theta_4(x,t)\right) \tag{5}$$

The longitudinal interlayer shear stress between rail II and bridge can be expressed as follows

$$\varsigma_2=k_{s2}\zeta_2(x,t)=k_{s2}\left[h_r\theta_2(x,t)+h_b\theta_4(x,t)\right] \tag{6}$$

where, h_b is half of the transverse cross-section height of bridge; θ_2 (x, t) and θ_4 (x, t) are the cross-section angle of rail II and bridge, respectively; k_{s2} is the interlayer slip stiffness of rail II and bridge.

The longitudinal displacement of each point at the cross-section of rail I and rail III can be expressed as follows

$$u_1=-z\theta_1, \qquad u_3=-z\theta_3 \tag{7}$$

where, z is the distance from each point at the cross-section to the central axis of cross-section.

Using Formula (7), the strain and stress of each point at the cross-section of rail I and rail III can be expressed as follows

$$\begin{cases}\varepsilon_{z1}=-z\dfrac{\partial\theta_1}{\partial x},\sigma_{z1}=-E_1z\dfrac{\partial\theta_1}{\partial x}\\ \varepsilon_{z3}=-z\dfrac{\partial\theta_3}{\partial x},\sigma_{z3}=-E_3z\dfrac{\partial\theta_3}{\partial x}\end{cases} \tag{8}$$

Shear strain and shear stress of rail I and rail III can be expressed as follows

$$\begin{cases}\gamma_{xz1}=\dfrac{\partial w_1}{\partial x}-\theta_1,\tau_{xz1}=G_1\left[\dfrac{\partial w_1}{\partial x}-\theta_1\right]\\ \gamma_{xz3}=\dfrac{\partial w_3}{\partial x}-\theta_3,\tau_{xz3}=G_3\left[\dfrac{\partial w_3}{\partial x}-\theta_3\right]\end{cases} \tag{9}$$

where, E_1, E_3 and G_1, G_3 are the elasticity modulus and shear modulus of rail, respectively.

The longitudinal displacement of each point at the cross-section of bridge and rail II can be expressed as follows

$$u_i=-z\theta_i \quad i=2,4 \tag{10}$$

Using Formula (10), the strain and stress of each point at the cross-section of bridge and rail II can be expressed as follows (Lai *et al*. 2019)

$$\varepsilon_{zi}=-z\frac{\partial\theta_i}{\partial x}, \quad \sigma_{zi}=-E_iz\frac{\partial\theta_i}{\partial x}, \qquad i=2,4 \tag{11}$$

The shear strain and shear stress of bridge and rail II can be expressed as follows

$$\gamma_{xzi}=\frac{\partial w_i}{\partial x}-\theta_i, \quad \tau_{xzi}=G_i\frac{\partial w_i}{\partial x}-G_i\theta_i, \qquad i=2,4 \tag{12}$$

where, E_i (i = 2, 4) and G_i (i = 2, 4) are the elasticity modulus and shear modulus of rail II and bridge, respectively, i.e., $E_1=E_2=E_3$ and $G_1=G_2=G_3$.

2.2 Strain energy and kinetic energy of HSRBTS

The strain energy of rail I can be expressed as follows

$$V_1=\frac{1}{2}\int_{L_1}\left[\int_{A_1}\left(\sigma_{z1}\varepsilon_{z1}+\tau_{xz1}r_{xz1}\right)dA+\vartheta_1w_1+\varsigma_1\zeta_1\right]dx \tag{13}$$

By substituting Formulas (7)-(9) into Formula (13), the following equation can be obtained

$$V_1=\frac{1}{2}\int_{L_1}\begin{bmatrix}E_1I_{y1}\theta_1'^2+G_1A_1\left(w_1'-\theta_1\right)^2+k_1w_1^2\\+k_{s1}h_r^2\theta_1^2\end{bmatrix}dx \tag{14}$$

The kinetic energy of rail in a track system by considering the effect of rotational inertia can be expressed as follows

$$T_1=\frac{1}{2}\int_{L_1}m_1\dot{w}_1^2dx+\frac{1}{2}\int_{L_1}\int_{A_1}\rho_1\dot{u}_1^2dAdx \tag{15}$$

Further, the following equation can be obtained

$$T_1=\frac{1}{2}\int_{L_1}\left(m_1\dot{w}_1^2+\rho_1I_{y1}\dot{\theta}_1^2\right)dx \tag{16}$$

where, $I_{y1}=\int_{A_1}z^2dA$; A_1 is the cross-sectional area of the rail; $m_1=\rho_1A_1$ is the areic mass of rail; ρ_1 is the density of rail; L_1 is the length of rail at the subgrade section.

Similarly, the strain of rail III can be expressed as follows

$$V_3=\frac{1}{2}\int_{L_3}\begin{bmatrix}E_3I_{y3}\theta_3'^2+G_3A_3\left(w_3'-\theta_3\right)^2+k_3w_3^2\\+k_{s3}h_r^2\theta_3^2\end{bmatrix}dx \tag{17}$$

The kinetic energy of rail III is

$$T_3=\frac{1}{2}\int_{L_3}\left(m_3\dot{w}_3^2+\rho_3I_{y3}\dot{\theta}_3^2\right)dx \tag{18}$$

where, $I_{y3}=\int_{A_3}z^2dA$; A_3 is the cross-sectional area of the rail; $m_3=\rho_3A_3$ is the areic mass of rail; ρ_3 is the density of rail, $\rho_3=\rho_1$; L_3 is the length of rail at subgrade section.

The total strain energy of rail II and bridge can be expressed as follows

$$V_2=\frac{1}{2}\int_{L_2}\begin{bmatrix}E_2I_{y2}\theta_2'^2+G_2A_2\left(w_2'-\theta_2\right)^2+\\E_4I_{y4}\theta_4'^2+G_4A_4\left(w_4'-\theta_4\right)^2\\+k_2\left(w_2-w_4\right)^2+\varsigma_2\zeta_2\end{bmatrix}dx \tag{19}$$

The total kinetic energy of rail II and bridge can be expressed as follows

$$T_2 = \frac{1}{2}\int_{L_2}\left(m_2\dot{w}_2^{\,2} + m_4\dot{w}_4^{\,2} + \rho_1 I_{y2}\dot{\theta}_2^{\,2} + \rho_4 I_{y4}\dot{\theta}_4^{\,2}\right)dx \quad (20)$$

where, $I_{yi} = \int_{A_1} z^2 dA$ (i = 2, 4); $m_i = \rho_i A_i$ (i = 2, 4) and ρ_i (i = 2, 4) are the areic mass and density of rail and bridge, respectively; L_2 is the length of rail at the bridge section.

2.3 Vibration differential equation and boundary conditions of HSRBTS

Using the energy-variational principle $\delta\int_{t_0}^{t_1}(T_n - V_n)dt = 0$ (n = 1, 2, 3), the vibration differential equations and natural boundary conditions of bending vibration of rail I can be expressed as follows (Menasria *et al*. 2017)

$$E_1 I_{y1}\theta_1'' - \rho_1 I_{y1}\ddot{\theta}_1 + G_1 A_1\left(w_1' - \theta_1\right) - k_{s1}h_r^{\,2}\theta_1 = 0 \quad (21)$$

$$-m_1\ddot{w}_1 + G_1 A_1\left(w_1'' - \theta_1'\right) - k_1 w_1 = 0 \quad (22)$$

$$E_1 I_{y1}\theta_1'\delta\theta_1\big|_0 = 0, \quad G_1 A_1\left(w_1' - \theta_1\right)\delta w_1\big|_0 = 0 \quad (23)$$

$$E_1 I_{y1}\theta_1'\delta\theta_1\big|_{L_1} = 0, \quad G_1 A_1\left(w_1' - \theta_1\right)\delta w_1\big|_{L_1} = 0 \quad (24)$$

Similarly, the vibration differential equations and natural boundary conditions of bending vibration of rail III can be expressed as follows

$$E_3 I_{y3}\theta_3'' - \rho_1 I_{y3}\ddot{\theta}_3 + G_3 A_3\left(w_3' - \theta_3\right) - k_{s3}h_r^{\,2}\theta_3 = 0 \quad (25)$$

$$-m_3\ddot{w}_3 + G_3 A_3\left(w_3'' - \theta_3'\right) - k_3 w_3 = 0 \quad (26)$$

$$E_3 I_{y3}\theta_3'\delta\theta_3\big|_0 = 0, \quad G_3 A_3\left(w_3' - \theta_3\right)\delta w_3\big|_0 = 0 \quad (27)$$

$$E_3 I_{y3}\theta_3'\delta\theta_3\big|_{L_3} = 0, \quad G_3 A_3\left(w_3' - \theta_3\right)\delta w_3\big|_{L_3} = 0 \quad (28)$$

The vibration differential equations and natural boundary conditions of bending vibration of rail II and bridge can be expressed as follows

$$-m_2\ddot{w}_2 + G_2 A_2\left(w_2'' - \theta_2'\right) - k_2\left(w_2 - w_4\right) = 0 \quad (29)$$

$$\begin{aligned}-\rho_1 I_{y2}\ddot{\theta}_2 &+ E_2 I_{y2}\theta_2'' + G_2 A_2\left(w_2' - \theta_2\right)\\ &- k_{s2}\left(h_r\theta_2 + h_b\theta_4\right)h_r = 0\end{aligned} \quad (30)$$

$$\begin{aligned}-\rho_4 I_{y4}\ddot{\theta}_4 &+ E_4 I_{y4}\theta_4'' + G_4 A_4\left(w_4' - \theta_4\right)\\ &- k_{s2}\left(h_r\theta_2 + h_b\theta_4\right)h_b = 0\end{aligned} \quad (31)$$

$$-m_4\ddot{w}_4 + G_4 A_4\left(w_4'' - \theta_4'\right) + k_2\left(w_2 - w_4\right) = 0 \quad (32)$$

$$E_2 I_{y2}\theta_2'\delta\theta_2\big|_0 = 0, \quad E_4 I_{y4}\theta_4'\delta\theta_4\big|_0 = 0 \quad (33)$$

$$G_2 A_2\left(w_2' - \theta_2\right)\delta w_2\big|_0 = 0, \quad G_4 A_4\left(w_4' - \theta_4\right)\delta w_4\big|_0 = 0 \quad (34)$$

$$E_2 I_{y2}\theta_2'\delta\theta_2\big|_{L_2} = 0, \quad E_4 I_{y4}\theta_4'\delta\theta_4\big|_{L_2} = 0 \quad (35)$$

$$G_2 A_2\left(w_2' - \theta_2\right)\delta w_2\big|_{L_2} = 0, \quad G_4 A_4\left(w_4' - \theta_4\right)\delta w_4\big|_{L_2} = 0 \quad (36)$$

3. Solving natural vibration frequency of HSRBTS

3.1 Solving variation differential equations

Let

$$\theta_j\left(x,t\right) = \theta_{j1}\left(x\right)\sin\left(\omega t + \varphi\right) \quad \left(j = 1,2,3,4\right) \quad (37)$$

$$w_j\left(x,t\right) = w_{j1}\left(x\right)\sin\left(\omega t + \varphi\right) \quad \left(j = 1,2,3,4\right) \quad (38)$$

$$d^k = \frac{\partial^k}{\partial x^k} \quad (39)$$

By substituting Formulas (37)-(39) into Formulas (21), (22), (25), (26) and (29)-(32), and reorganizing the result, the following equations can be obtained

$$\left(E_1 I_{y1}d^2 + \omega^2\rho_1 I_{y1} - G_1 A_1 - k_{s1}h_r^{\,2}\right)\theta_{11} + G_1 A_1 d w_{11} = 0 \quad (40)$$

$$-G_1 A_1 d\theta_{11} + \left(\omega^2 m_1 + G_1 A_1 d^2 - k_1\right)w_{11} = 0 \quad (41)$$

$$\begin{aligned}\left(\omega^2\rho_1 I_{y2} + E_2 I_{y2}d^2 - G_2 A_2 - k_{s2}h_r h_r\right)\theta_{21} +\\ G_2 A_2 d w_{21} - k_{s2}h_r h_b\theta_{41} = 0\end{aligned} \quad (42)$$

$$\left(\omega^2 m_2 + G_2 A_2 d^2 - k_2\right)w_{21} - G_2 A_2 d\theta_{21} + k_2 w_{41} = 0 \quad (43)$$

$$\begin{aligned}\left(\omega^2\rho_4 I_{y4} + E_4 I_{y4}d^2 - G_4 A_4 - k_{s2}h_b h_b\right)\theta_{41} -\\ k_{s2}h_r h_b\theta_{21} + G_4 A_4 d w_{41} = 0\end{aligned} \quad (44)$$

$$\left(\omega^2 m_4 + G_4 A_4 d^2 - k_2\right)w_{41} - G_4 A_4 d\theta_{41} + k_2 w_{21} = 0 \quad (45)$$

$$\left(E_3 I_{y3}d^2 + \omega^2\rho_1 I_{y3} - G_3 A_3 - k_{s3}h_r^{\,2}\right)\theta_{31} + G_3 A_3 d w_{31} = 0 \quad (46)$$

$$\left(\omega^2 m_3 + G_3 A_3 d^2 - k_3\right)w_{31} - G_3 A_3 d\theta_{31} = 0 \quad (47)$$

The characteristic equations corresponding to the differential Eqs. (40)-(47) are as follows

$$\begin{vmatrix}\Re_{11} & \Re_{12}\\ \Re_{21} & \Re_{22}\end{vmatrix}U_1 = 0 \quad (48)$$

$$\begin{vmatrix} \Im_{11} & \Im_{12} & \Im_{13} & 0 \\ \Im_{21} & \Im_{22} & 0 & \Im_{24} \\ \Im_{31} & 0 & \Im_{33} & \Im_{34} \\ 0 & \Im_{42} & \Im_{43} & \Im_{44} \end{vmatrix} U_2 = 0 \tag{49}$$

$$\begin{vmatrix} \wp_{11} & \wp_{12} \\ \wp_{21} & \wp_{22} \end{vmatrix} U_3 = 0 \tag{50}$$

where, $|\,|$ is the matrix determinant, $\Re_{12} = G_1 A_1 d$, $\Re_{11} = E_1 I_{y1} d^2 + \omega^2 \rho_1 I_{y1} - G_1 A_1 - k_{s1} h_r^2$, $\Re_{21} = -G_1 A_1 d$, $\Re_{22} = \omega^2 m_1 + G_1 A_1 d^2 - k_1$, $\Im_{13} = -k_{s2} h_r h_b$, $\Im_{12} = G_2 A_2 d$, $\Im_{11} = \omega^2 \rho_1 I_{y2} + E_2 I_{y2} d^2 - G_2 A_2 - k_{s2} h_r h_r$, $\Im_{21} = -G_2 A_2 d$, $\Im_{22} = \omega^2 m_2 + G_2 A_2 d^2 - k_2$, $\Im_{24} = k_2$, $\Im_{34} = G_4 A_4 d$, $\Im_{33} = \omega^2 \rho_4 I_{y4} + E_4 I_{y4} d^2 - G_4 A_4 - k_{s2} h_b h_b$, $\Im_{31} = -k_{s2} h_r h_b$, $\Im_{42} = k_2$, $\Im_{43} = -G_4 A_4 d$, $\wp_{12} = G_3 A_3 d$, $\wp_{21} = -G_3 A_3 d$, $\Im_{44} = \omega^2 m_4 + G_4 A_4 d^2 - k_2$, $\wp_{22} = \omega^2 m_3 + G_3 A_3 d^2 - k_3$, $\wp_{11} = E_3 I_{y3} d^2 + \omega^2 \rho_1 I_{y3} - G_3 A_3 - k_{s3} h_r^2$.

By analyzing Formulas (48)-(50), the forms of solution of characteristic equations are as follows

$$d_{1,2} = \pm(\beta_1 + \gamma_1 i), \qquad d_{3,4} = \pm(\beta_2 + \gamma_2 i) \tag{51}$$

$$\begin{cases} d_{5,6} = \pm(\eta_1 + \gamma_1 i), d_{7,8} = \pm(\eta_2 + \gamma_2 i) \\ d_{9,10} = \pm(\eta_3 + \gamma_3 i), d_{11,12} = \pm(\eta_4 + \gamma_4 i) \end{cases} \tag{52}$$

$$d_{13,14} = \pm(\chi_1 + \gamma_1 i), \qquad d_{15,16} = \pm(\chi_2 + \gamma_2 i) \tag{53}$$

Then, the solutions of equation sets (40)-(47) can be expressed as follows

$$\begin{aligned} \theta_{11}(x) &= \sum_{i=1}^{4} a_i \beta_{1i} \exp(d_i x), \\ w_{11}(x) &= \sum_{i=1}^{4} a_i \beta_{2i} \exp(d_i x) \end{aligned} \tag{54}$$

$$\begin{aligned} \theta_{21}(x) &= \sum_{i=5}^{12} a_i \eta_{1i} \exp(d_i x), \\ w_{21}(x) &= \sum_{i=5}^{12} a_i \eta_{2i} \exp(d_i x) \end{aligned} \tag{55}$$

$$\begin{aligned} \theta_{41}(x) &= \sum_{i=5}^{12} a_i \eta_{3i} \exp(d_i x), \\ w_{41}(x) &= \sum_{i=5}^{12} a_i \eta_{4i} \exp(d_i x) \end{aligned} \tag{56}$$

$$\begin{aligned} \theta_{31}(x) &= \sum_{i=13}^{16} a_i \chi_{1i} \exp(d_i x), \\ w_{31}(x) &= \sum_{i=13}^{16} a_i \chi_{2i} \exp(d_i x) \end{aligned} \tag{57}$$

$$\beta_{1i} = -\frac{\Re_{12}}{\Re_{11}} \quad i = 1,2,3,4 \tag{58}$$

$$\beta_{2i} = 1 \quad i = 1,2,3,4 \tag{59}$$

$$\eta_{1i} = \frac{\left(\frac{\Im_{24}\Im_{12}}{\Im_{22}} + \frac{\Im_{34}\Im_{13}}{\Im_{33}}\right)}{\left(\Im_{11} - \frac{\Im_{21}\Im_{12}}{\Im_{22}} - \frac{\Im_{31}\Im_{13}}{\Im_{33}}\right)} \quad i = 5,6,\ldots,12 \tag{60}$$

$$\eta_{2i} = -\frac{\Im_{24}}{\Im_{22}} - \frac{\Im_{21}}{\Im_{22}}\left[\frac{\left(\frac{\Im_{24}\Im_{12}}{\Im_{22}} + \frac{\Im_{34}\Im_{13}}{\Im_{33}}\right)}{\left(\Im_{11} - \frac{\Im_{21}\Im_{12}}{\Im_{22}} - \frac{\Im_{31}\Im_{13}}{\Im_{33}}\right)}\right] \quad i = 5,6,\ldots,12 \tag{61}$$

$$\eta_{3i} = -\frac{\Im_{34}}{\Im_{33}} - \frac{\Im_{31}}{\Im_{33}}\left[\frac{\left(\frac{\Im_{24}\Im_{12}}{\Im_{22}} + \frac{\Im_{34}\Im_{13}}{\Im_{33}}\right)}{\left(\Im_{11} - \frac{\Im_{21}\Im_{12}}{\Im_{22}} - \frac{\Im_{31}\Im_{13}}{\Im_{33}}\right)}\right] \quad i = 5,6,\ldots,12 \tag{62}$$

$$\eta_{4i} = 1 \quad i = 5,6,\ldots,12 \tag{63}$$

$$\chi_{1i} = -\frac{\wp_{12}}{\wp_{11}} \quad i = 13,14,15,16 \tag{64}$$

$$\chi_{2i} = 1 \quad i = 13,14,15,16 \tag{65}$$

where, a_i (i = 1, 2,..., 16) is the integration constant.

3.2 Processing boundary conditions

According to the Saint-Venant principle (Qin *et al.* 2017), after the rail at the subgrade section reaches a certain length, the boundary conditions of the left end of rail I and the right end of rail III have a relatively slight effect on the dynamic characteristics of bridge-track system. Therefore, to simplify the calculation, it was assumed that the two boundary conditions in this paper are simple support, and its mathematical relationship can be expressed as follows

$$\theta'_{11}\big|_0 = 0, \qquad w_{11}\big|_0 = 0 \tag{66}$$

$$\theta'_{31}\big|_{L_3} = 0, \qquad w_{31}\big|_{L_3} = 0 \tag{67}$$

According to displacement coordination of rail I and rail II, the following equations can be obtained

$$\theta_1\big|_{x=L_1} = \theta_2\big|_{x=0}, \qquad w_1\big|_{x=L_1} = w_2\big|_{x=0} \tag{68}$$

According to mechanical coordination of rail I and rail II, the following equations can be obtained

$$E_2 I_{y2} \theta'_2\big|_0 - E_1 I_{y1} \theta'_1\big|_{L_1} = 0 \tag{69}$$

Table 1 Comparison of calculation results of natural vibration frequencies of HSRBTS of 24 m

Mode	Calculation methods			E_f (%)	E_m (%)	E_a (%)
	Analytic method (Hz)	ANSYS(Hz)	MIDAS(Hz)			
1st	5.676	5.676	5.688	0.21	-0.21	0.94
2nd	21.986	21.986	22.152	0.76	-0.75	-0.10
3rd	42.170	42.170	42.832	1.57	-1.54	0.01
4th	42.824	42.824	42.897	0.17	-0.17	-0.03
5th	42.828	42.828	42.958	0.30	-0.30	1.08
6th	42.891	42.891	43.404	1.20	-1.18	1.30

Table 2 Comparison of calculation results of natural vibration frequencies of HSRBTS of 32 m

Mode	Calculation methods			E_f (%)	E_m (%)	E_a (%)
	Analytic method (Hz)	ANSYS(Hz)	MIDAS(Hz)			
1st	3.183	3.214	3.209	0.16	-0.96	-0.80
2nd	12.573	12.644	12.598	0.36	-0.56	-0.20
3rd	27.534	27.745	27.473	0.99	-0.76	0.22
4th	42.813	42.821	42.824	-0.01	-0.02	-0.03
5th	43.290	42.871	42.828	0.10	0.98	1.08
6th	43.449	42.897	42.890	0.02	1.29	1.30

$$G_2A_2\left(w_2'-\theta_2\right)\Big|_0-G_1A_1\left(w_1'-\theta_1\right)\Big|_{L_1}=0 \tag{70}$$

According to the displacement coordination of rail III and rail II, the following equations can be obtained

$$\theta_2\Big|_{x=L_2}=\theta_3\Big|_{x=0}\ ,\qquad w_2\Big|_{x=L_2}=w_3\Big|_{x=0} \tag{71}$$

According to the mechanical coordination of rail III and rail II, the following equations can be obtained

$$E_3I_{y3}\theta_3'\Big|_0-E_2I_{y2}\theta_2'\Big|_{L_2}=0 \tag{72}$$

$$G_3A_3\left(w_3'-\theta_3\right)\Big|_0-G_2A_2\left(w_2'-\theta_2\right)\Big|_{L_2}=0 \tag{73}$$

Boundary conditions for both ends of the bridge can be expressed as follows

$$\theta_{41}'\Big|_0=0,\quad \theta_{41}'\Big|_{L_2}=0,\quad w_{41}\Big|_0=0,\quad w_{41}\Big|_{L_2}=0 \tag{74}$$

3.3 Solving natural vibration frequency

By substituting Formulas (54)-(57) into Formulas (66)-(74), the effect of linear algebraic equations of HSRBTS on integration constant can be expressed as follows

$$\left[B(\omega)\right]\left\{a_1,a_2,...,a_{16}\right\}^T=0 \tag{75}$$

If the system of equations requires untrivial solutions, then only the following should be met

$$\left|B(\omega)\right|=0 \tag{76}$$

By solving the Eq. (76), natural vibration frequency of HSRBTS ω_i (i = 1, 2,.....) can be obtained.

4. Verification and application

4.1 Example analysis and verification

To verify the rationality of analytic method proposed in this paper, two typical examples of HSRBTS were selected (Sun *et al*. 2015, Kang *et al*. 2017). Their physical dimension and mechanical parameters are as follows (Lai and Ho 2016): The spans of simply supported beam bridge of the two examples are 24 m and 32 m. Thereinto, the spans of 24 m and 32 m are the relatively economic and reasonable spans, which are the main and commonly used spans in the railways (Ministry of Railways 2014, 2017). The elasticity modulus of the beam bridge is 3.45×10^4 N/mm^2, and the density of the beam bridge is 2549 kg/m^3. The rails in the two examples are both jointless rails of 60 kg/m. The rail lengths of the two examples at the subgrade section are 88 m and 96 m. The elasticity modulus of the rails is 2.06×10^5 N/mm^2, and the density of the rails is 7850 kg/m^3. The vertical interlayer compressive stiffness is k_1 = k_2 = k_3 = k = 6e7N/m, and the longitudinal interlayer slip stiffness is k_{s1} = k_{s2} = k_{s3} = k_s = 4.327e6 N/m. To verify the validity and rationality of the analytic method proposed in this paper, two types of finite-element analysis software MIDAS and ANSYS were used to establish a numerical simulation model for HSRBTS, and the numerical results for the first 6-order natural vibration frequency of HSRBTS were compared with the analytic calculation results of analytic method reported in this paper. In two numerical simulation models, the track system and major beam are

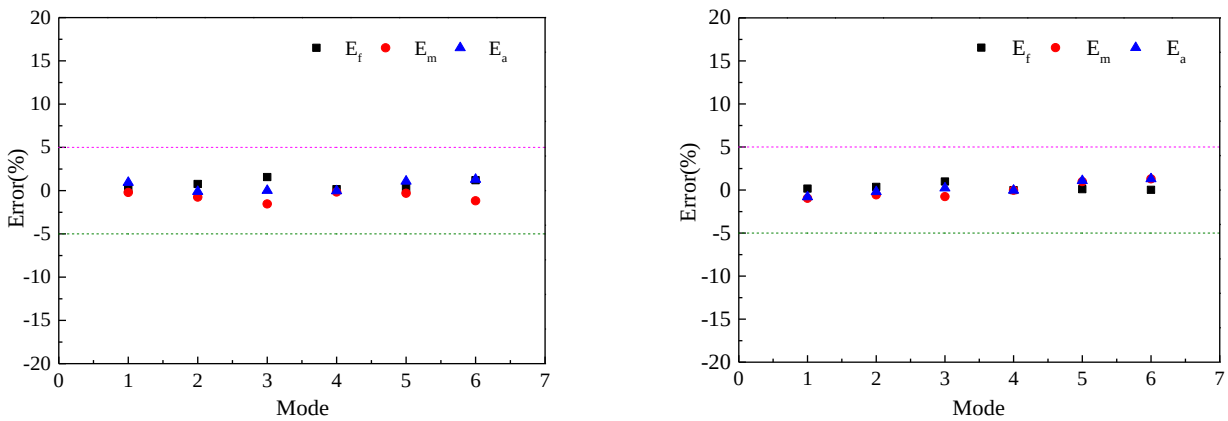

(a) HSRBTS of 24 m (b) HSRBTS of 32 m

Fig. 2 Comparison of calculation results error of natural vibration frequency of HSRBTS of 24 m and 32 m

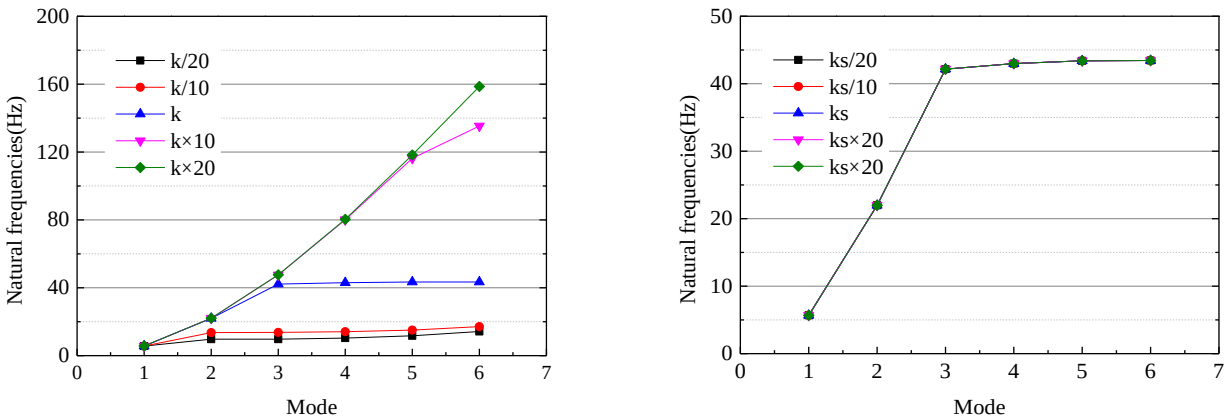

(a) Vertical interlayer compressive stiffness (b) Longitudinal interlayer slip stiffness

Fig. 3 The influence of interlayer stiffness on natural vibration characteristics of HSRBTS of 24 m

simulated by beam element, the interlayer components are simulated by spring element, and the subgrade is simulated by a series of continuous boundary. Standard hollow box beam section is used for bridge cross-section, for simplification, the width and thickness of the upper, bottom flange is 12 m and 0.6 m, 5 m and 0.4 m, respectively; and the height and thickness of web is 2.4 m and 0.6 m, respectively (Ministry of Railways 2017). The comparison results are shown in Tables 1-2 and Fig. 2. In the Tables, $E_f = (R_m - R_a) / R_a \times 100\%$ is the error of natural vibration frequency calculated through MIDAS (R_m) and ANSYS (R_a); $E_m = (R_m - R_{am}) / R_{am} \times 100\%$ is the error of natural vibration frequency calculated through MIDAS (R_m) and analytic method (R_{am}); $E_a = (R_a - R_{am}) / R_{am} \times 100\%$ is the error of natural vibration frequency calculated through ANSYS and analytic method (R_{am}).

It can be seen from Tables 1-2 and Fig. 2 that: the analytic method proposed in this paper, ANSYS and MIDAS finite element methods in the calculation of the first 6-order natural vibration frequencies are in good agreement with each other. Moreover, the error between each other does not exceed 2%, which proves the accuracy of the analytic method proposed in this paper.

4.2 Method application

4.2.1 Effect of interlayer stiffness and length of rail at subgrade section on the natural vibration characteristics of HSRBTS

The vertical interlayer compressive stiffness and longitudinal interlayer slip stiffness of rail and bridge were changed; the values taken for vertical interlayer compressive stiffness being $k/20$, $k/10$, k, $10k$, and $20k$, respectively, and those for longitudinal interlayer slip stiffness being $k_S/20$, $k_S/10$, k_S, $10k_S$, and $20k_S$, respectively (Lee 2011). Then, the analytic method proposed in this paper was used to calculate the natural vibration characteristics of HSRBTS under different interlayer stiffness to study the influencing trends of interlayer stiffness on the natural vibration characteristics of this system. The calculation results are shown in Figs. 3 and 4.

Figs. 3 and 4 show that the longitudinal interlayer slip stiffness has a relatively slight effect on the natural vibration frequency of both 24 m and 32 m HSRBTS. This indicates that in the vibration modes of HSRBTS, both the rail and main beam are dominated by bending deflection, and shear deformation plays a relatively small role. The vertical interlayer compressive stiffness has a relatively

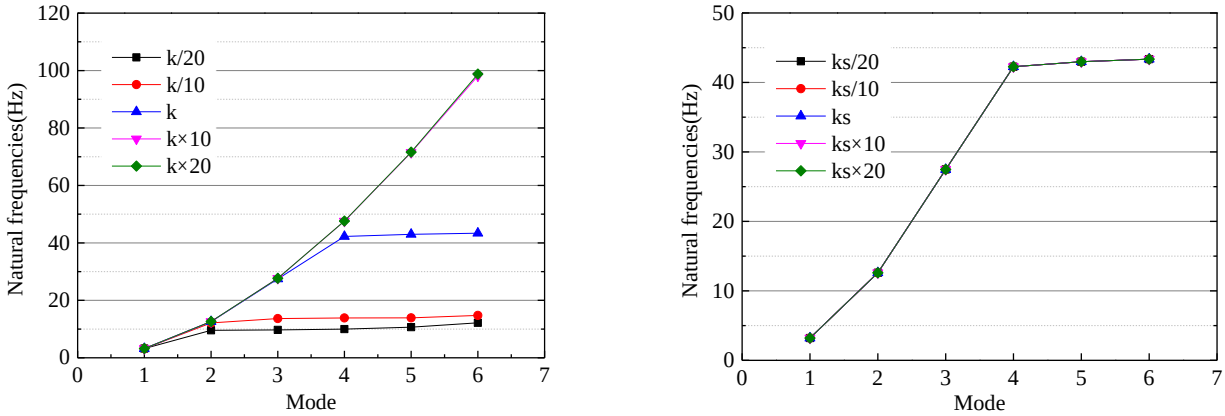

(a) Vertical interlayer compressive stiffness (b) Longitudinal interlayer slip stiffness

Fig. 4 The influence of interlayer stiffness on natural vibration characteristics of HSRBTS of 32 m

slight effect on the low-order natural vibration frequency of 24 m and 32 m HSRBTS, but has a relatively significant effect on high-order natural vibration frequency. This is mainly because the low-order mode of the system is dominated by the coupling vibration of bridge-track system. However, the stiffness and mass of rail are both smaller than those of the bridge, and the effect of vertical compressive stiffness plays a minor role.

To study the effect of rail length at the subgrade section on the natural vibration characteristics of HSRBTS, the analytic calculation method proposed in this paper was used to calculate the natural vibration frequencies of HSRBTS with the rail length at the subgrade section being 1 m, 5 m, 10 m, 50 m, 100 m, and 200 m, respectively. The calculation results are shown in Fig. 5. Fig. 5 shows that the natural vibration frequencies of HSRBTS decreases with the increase in rail length at the subgrade section, and with the increase in rail length at the subgrade section, the natural vibration frequencies of HSRBTS became stable. This indicates that when the rail length at the subgrade section is relatively small, the length of subgrade section has a certain effect on the natural vibration characteristics of HSRBTS, but when it is larger than a certain critical value, the effect of length of subgrade section on the natural vibration characteristics of HSRBTS can be ignored.

4.2.2 Critical length of rail at subgrade section for HSRBTS

From the above analysis, it can be concluded that vertical interlayer compressive stiffness and the rail length at the subgrade section have a certain effect on the vibration characteristics of HSRBTS (Sun *et al*. 2016). The analytic method proposed in this paper was used to calculate the natural vibration characteristics of HSRBTS under different vertical compressive stiffness and length of rail at subgrade section. By taking the natural vibration frequencies of the first-10 order as the research object, this study evaluated the effect of different rail length at the subgrade section on the natural vibration characteristics of HSRBTS with different vertical interlayer compressive stiffness and calculated the critical rail length at the subgrade section when the natural variation frequency of HSRBTS became stable under different vertical interlayer compressive stiffnesses (Mirza *et al*. 2016). The calculation results are shown in Table 3.

Table 3 shows that under different vertical interlayer compressive stiffnesses, the rail at the subgrade section for HSRBTS has a critical length, and the critical length of rail at the subgrade section for HSRBTS decreases with the increase in vertical interlayer compressive stiffness. This is because the higher the vertical interlayer compressive stiffness for HSRBTS, the stronger the restriction effect of

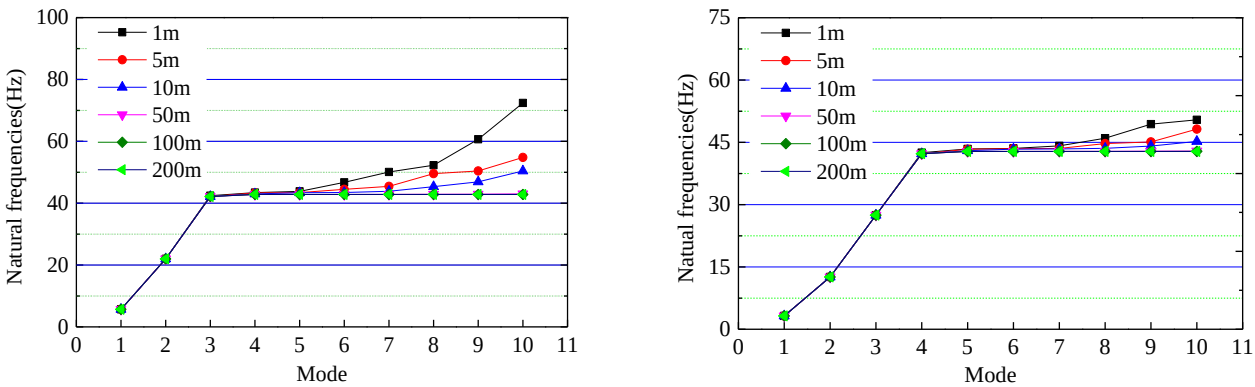

(a) Vertical interlayer compressive stiffness (b) Longitudinal interlayer slip stiffness

Fig. 4 The influence of interlayer stiffness on natural vibration characteristics of HSRBTS of 32 m

Table 3 Critical length of rail at the subgrade section (m)

Bridge span(m)	*k*/20	*k*/10	*k*	10*k*	20*k*
24	240	200	170	60	40
32	220	180	150	40	20

rail in the subgrade section, and the smaller the critical length of rail at the subgrade section.

5. Conclusions

Based on the energy-variational principle, the vibration differential equations and natural boundary conditions for HSRBTS considering the interlayer slip effect were derived; furthermore, an analytic calculation method for the natural vibration frequencies of HSRBTS was obtained. The analytic method obtained in this study was used to calculate the natural vibration characteristics of HSRBTS examples under different vertical compressive stiffnesses and rail lengths at the subgrade section, and the variation trends of natural vibration frequencies of HSRBTS with the variation in interlayer stiffness and rail length at the subgrade section were obtained. The following conclusions are drawn:

- The calculation results obtained from the analytic method proposed in this paper agree well with the calculation results obtained from MIDAS and ANSYS numerical methods, thus validating the analytic method proposed in this paper.
- The vertical interlayer compressive stiffness has a relatively slight effect on the low-order natural vibration frequency of the HSRBTS, but has a greater effect on the high-order natural vibration frequency.
- In the vibration mode of HSRBTS, both the rail and main beam are dominated by the bending deflection with shear deformation playing a relatively small role. The effect of longitudinal interlayer slip stiffness on the natural vibration frequency of HSRBTS can be ignored.
- The natural vibration frequency of HSRBTS decreases with the increase in the rail length at the subgrade section, and with the increase in the rail length at the subgrade section, the natural vibration frequency of HSRBTS becomes stable.
- Under different vertical interlayer compressive stiffness conditions, the subgrade section of HSRBTS has a critical rail length, and the critical length of rail at subgrade section decreases with the increase in vertical interlayer compressive stiffness.

Acknowledgments

The research described in this paper was financially supported by the National Natural Science Foundations of China (51408449, 51778630), the Innovation-driven Plan in Central South University under grant (2015CX006), the Fundamental Research Funds for the Central Universities of Central South University (2018zzts189).

References

Bian, X., Cheng, C., Jiang, J., Chen, R. and Chen, Y. (2016), "Numerical analysis of soil vibrations due to trains moving at critical speed", *Acta Geotech*, **11**(2), 281-294.

Bucinskas, P., Andersen, L.V. and Persson, K. (2016), "Numerical modelling of ground vibration caused by elevated high-speed railway lines considering structure-soil-structure interaction", *International Congress and Exposition on Noise Control Engineering, Inter-Noise*.

Connolly, D.P., Marecki, G.P., Kouroussis, G., Thalassinakis, I. and Woodward, P.K. (2016), "The growth of railway ground vibration problems-A review", *Sci. Total Environ.*, **568** 1276-1282.

Gao, Y., Huang, H., Ho, C.L. and Judge, A. (2016), "Field validation of a three-dimensional dynamic track-subgrade interaction model", *Proceedings of the Institution of Mechanical Engineers, Part F: Journal of Rail and Rapid Transit*, **232**(1), 130-143.

Hou, Z., Xia, H. and Wang Y.E.A. (2015), "Dynamic analysis and model test on steel-concrete composite beams under moving loads", *Steel Compos. Struct., Int. J.*, **18**(3), 565-582. http://dx.doi.org/10.12989/scs.2015.18.3.565

Hu, J., Bian, X. and Jiang, J. (2016), "Critical velocity of high-speed train running on soft soil and induced dynamic soil response", *Procedia Engineering*, **143**, 1034-1042.

Kang, X., Jiang, L., Bai, Y. and Caprani, C.C. (2017), "Seismic damage evaluation of high-speed railway bridge components under different intensities of earthquake excitations", *Eng. Struct.*, **152** 116-128.

Kimani, S.K. and Kaewunruen, S. (2017), "Free vibrations of precast modular steel-concrete composite railway track slabs", *Steel Compos. Struct., Int. J.*, **24**(1), 113-128. http://dx.doi.org/10.12989/scs.2017.24.1.113

Kun, L., Lei, X. and Zeng, S. (2017), "Influence analysis on the effect of rail fastening parameters on the vibration response of track-bridge system", *Adv. Mech. Eng.*, **9**(8), 2071939371.

Lai, M.H. and Ho, J.C.M. (2016), "A theoretical axial stress-strain model for circular concrete-filled-steel-tube columns", *Eng. Struct.*, **125**, 124-143.

Lai, M., Hanzic, L., and Ho, J. (2019), "Fillers to improve passing ability of concrete", *Struct. Concrete*, **20**(1), 185-197.

Lee, I.W. (2011), "Dynamic response characteristics for two-layered trackbed structure by train load (열차하중에 의한이층노반구조의동적응답특성)", *J. Kor. Soc. Railway* (*한국철도학회논문집*), **14**(2), 160-166.

Lei, X. and Rose, J.G. (2008), "Numerical investigation of vibration reduction of ballast track with asphalt trackbed over soft subgrade", *.J Vib. Control*, **14**(12), 1885-1902.

Lei, X. and Zhang, B. (2011), "Analysis of dynamic behavior for slab track of high-speed railway based on vehicle and track elements", *J. Transp. Eng.*, **137**(4), 227-240.

Li, X., Liang, L. and Wang, D. (2018), "Vibration and noise characteristics of an elevated box girder paved with different track structures", *J. Sound Vib.*, **425** 21-40.

Liu, W., Dai, G., Yu, Z., Chen, Y.F. and He, X. (2018), "Interaction between continuous welded rail and long-span steel truss arch bridge of a high-speed railway under seismic action", *Struct. Infras. E*, **14**(8), 1051-1064.

Luo, W. and Lei, X. (2014), "Analysis of dynamic behavior for ballastless track-bridge with a hybrid method", *Intel. Autom. Soft Co.*, **20**(4), 487-500.

Menasria, A., Bouhadra, A. and Tounsi, A. (2017), "A new and simple HSDT for thermal stability analysis of FG sandwich plates", *Steel Compos. Struct., Int. J.*, **25**(2), 157-175. http://dx.doi.org/10.12989/scs.2017.25.2.157

Ministry of Railways (2014), TB10621. Code for Design high

speed railway, China Railway Press, Beijing, China. [In Chinese)

Ministry of Railways (2017), TB10002. Code for design on railway bridge and culvert", China Railway Press, Beijing, China. [In Chinese]

Mirza, O., Kaewunruen, S. and Kwok, K. (2016), "Design and modelling of pre-cast steel-concrete composites for resilient railway track slabs", *Steel Compos. Struct., Int. J.*, **22**(3), 537-565. http://dx.doi.org/10.12989/scs.2016.22.3.537

Qin, Y., Lu, J.Y., Huang, L.C.X. and Cao, S. (2017), "Flexural behavior of beams in steel plate shear walls", *Steel Compos. Struct., Int. J.*, **23**(4), 473-481. http://dx.doi.org/10.12989/scs.2017.23.4.473

Romero, A., Galvín, P. and Domínguez, J. (2012), "Comportamiento dinámico de viaductos cortos considerando la interacción vehículo-vía-estructura-suelo", *Revista Internacional de Métodos Numéricos para Cálculo y Diseño en Ingeniería*, **28**(1), 55-63.

Siekierski, W. (2016), "Analysis of concrete shrinkage along truss bridge with steel-concrete composite deck", *Steel Compos. Struct., Int. J.*, **20**(6), 1237-1257. http://dx.doi.org/10.12989/scs.2016.20.6.1237

Sun, W. (2014), "Random vibration analysis on vertical vehicle-track coupled system with timoshenko beam model", *J. Mech. Eng.*, **50**(18), 134. [In Chinese]

Sun, L., Hayashikawa, T., He, X. and Xie, W. (2015), "Influential parameter analysis on vibration responses of rigid-frame viaducts induced by running high-speed trains", *Int. J. Steel Struct.*, **15**(4), 809-826.

Sun, L.M., Xie, W.P., He, X.W. and Hayashikawa, T. (2016), "Prediction and mitigation analysis of ground vibration caused by running high-speed trains on rigid-frame viaducts", *Earthq. Eng. Eng. Vib.*, **15**(1), 31-47.

Toyooka, A., Ikeda, M. and Yanagawa, H.E.A. (2005), "Effects of track structure on seismic behavior of isolation system bridges", *Quarterly Report of RTRI*, **46**(4), 238-243.

Xie, X., Wang, Y. and Chen, L. (2012), "Effect of restrains on seismic response of cushioning railway bridges", *J. China Railway Soc.*, **34**(6). [In Chinese]

Yang, X.W. and He, Z.X. (2012), "Study on vibration characteristics of trapezoidal sleeper track", *J. Vib. Eng.*, **25**(4), 388-392.

Yang, Y.B. and Yau, J.D. (2017), "Resonance of high-speed trains moving over a series of simple or continuous beams with non-ballasted tracks", *Eng. Struct.*, **143**, 295-305.

Yang, X., Liu, X., Zhou, S., Ma, X., Shen, J. and Zang, J. (2016), "Vertical random vibration analysis of track-subgrade coupled system in high speed railway with pseudoexcitation method", *Shock Vib.*, **24**, 1-2.

Zhai, W.M. (2002), "New advance in vehicle-track coupling dynamics", *China Railway Sci.*, **23**(2), 1-14.

Zhang, J., Jia, H., Zheng, S. and Qin, S. (2016), "Analysis of a high-pier railway bridge under spatial stochastic stationary and non-stationary earthquake excitations", *Teh Vjesn*, **23**(2).

Zhu, Y., Li, X. and Jin, Z. (2016), "Three-dimensional random vibrations of a high-speed-train–bridge time-varying system with track irregularities", *Proceedings of the Institution of Mechanical Engineers, Part F: Journal of Rail and Rapid Transit*, **230**(8), 1851-1876.

CC

Nomenclature

The following symbols are used in this paper:

w_1	Vertical deflection of rail I
w_2	Vertical deflection of rail II
w_3	Vertical deflection of rail III
w_4	Vertical deflection of bridge
k_1	Vertical interlayer compressive stiffness between rail I and subgrade
k_2	Vertical interlayer compressive stiffness between rail II and bridge
k_3	Vertical interlayer compressive stiffness of rail III and subgrade
h_r	Half of the transverse cross-section height of the rail
θ_1	Cross-section angle of rail I
θ_2	Cross-section angle of rail II
θ_3	Cross-section angle of rail III
θ_4	Cross-section angle of bridge
k_{s1}	Longitudinal interlayer slip stiffness between rail I and subgrade
k_{s2}	Longitudinal interlayer slip stiffness of rail II and bridge
k_{s3}	Longitudinal interlayer slip stiffness between rail III and subgrade
h_b	Half of the transverse cross-section height of bridge
z	Distance from each point at the cross-section to the central axis of cross-section
A_i	Cross-sectional area of the rail and bridge
L_i	Length of rail at the subgrade and bridge section
E_i	Elasticity modulus of rail and bridge
G_i	Shear modulus of rail and bridge
m_i	Areic mass of rail and bridge
ρ_i	Density of rail and bridge
a_i	Integration constant